

# *EgoWorld*: Translating Exocentric View to Egocentric View using Rich Exocentric Observations

Junho Park<sup>1</sup>, Andrew Sangwoo Ye<sup>2</sup>, Taein Kwon<sup>3</sup>✉

<sup>1</sup>AI Lab, LG Electronics, <sup>2</sup>KAIST, <sup>3</sup>Visual Geometry Group, University of Oxford  
junho18.park@gmail.com, andyye@kaist.ac.kr, taein@robots.ox.ac.uk

<https://redorangeyellowy.github.io/EgoWorld/>

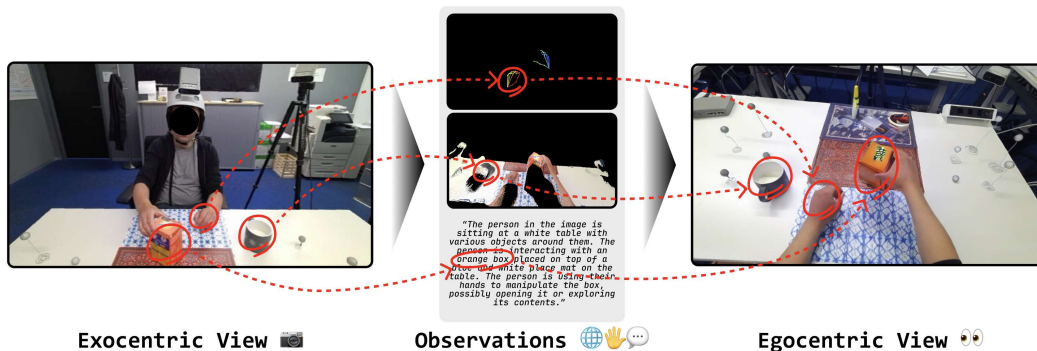


Figure 1: *EgoWorld* translates a single exocentric view into an egocentric view. By leveraging rich multimodal exocentric observations, such as projected point clouds, 3D hand poses, and textual descriptions, *EgoWorld* is able to generate high-quality egocentric views, even in unseen scenarios. Each observed modality provides complementary information that contributes to the accurate and realistic reconstruction of the egocentric view.

## Abstract

Egocentric vision is essential for both human and machine visual understanding, particularly in capturing the detailed hand-object interactions needed for manipulation tasks. Translating third-person views into first-person views significantly benefits augmented reality (AR), virtual reality (VR) and robotics applications. However, current exocentric-to-egocentric translation methods are limited by their dependence on 2D cues, synchronized multi-view settings, and unrealistic assumptions such as necessity of initial egocentric frame and relative camera poses during inference. To overcome these challenges, we introduce *EgoWorld*, a novel two-stage framework that reconstructs an egocentric view from rich exocentric observations, including projected point clouds, 3D hand poses, and textual descriptions. Our approach reconstructs a point cloud from estimated exocentric depth maps, reprojects it into the egocentric perspective, and then applies diffusion-based inpainting to produce dense, semantically coherent egocentric images. Evaluated on the H2O and TACO datasets, *EgoWorld* achieves state-of-the-art performance and demonstrates robust generalization to new objects, actions, scenes, and subjects. Moreover, *EgoWorld* shows promising results even on unlabeled real-world examples.

✉Corresponding author.

# 1 Introduction

Egocentric vision plays a crucial role in advancing visual understanding for both humans and intelligent systems [1–4]. Egocentric views are particularly valuable for capturing detailed hand-object interactions, which are essential in skill-intensive tasks such as cooking, assembling, or playing instruments. However, most existing resources are recorded from third-person perspectives, primarily due to the limited availability of head-mounted cameras and wearable recording devices. Consequently, the ability to generate or predict egocentric images from exocentric inputs holds significant promise for enhancing instructional videos and applications in augmented reality (AR), virtual reality (VR), and robotics, where perception is inherently egocentric. For example, instructional videos are often recorded from a third-person viewpoint, which can be challenging for viewers to follow due to the mismatched perspectives. Translating these videos into a first-person view enables more intuitive guidance by clearly showing detailed finger placements during a task. Moreover, this translation capability unlocks the development of robust, user-centered world models [5–7] that capture the spatial and temporal details necessary for real-time perception, planning, and interaction at scale.

Although exocentric-to-egocentric view translation holds great promise, it remains a particularly difficult challenge in computer vision. The main obstacle stems from the substantial visual and geometric differences between third-person and first-person views. Egocentric views focus on hands and objects with the fine detail necessary for precise manipulation, whereas exocentric views offer a wider context and kinematic cues but lack emphasis on these intricate interactions. Bridging these views is fundamentally under-constrained and cannot be addressed by geometric alignment alone, due to factors such as occlusions, restricted fields of view, and appearance changes across different viewpoints. For instance, elements like the inner pages of a book may be completely obscured in an exocentric perspective but still need to be realistically inferred in the egocentric output. Moreover, reconstructing background details in the egocentric view, which are invisible from the exocentric perspective, is nontrivial task.

Recently, the impressive achievements of diffusion models [8, 9] have opened up new possibilities for applying generative techniques to the task of exocentric-to-egocentric view translation. However, many existing approaches rely on restrictive input conditions, such as multi-view images [10], known relative camera pose [11], or a reference egocentric frame to generate subsequent ones [12], making them impractical for scenarios where only single view images are available. More closely, Exo2Ego [13] attempts to generate egocentric views from a single exocentric image. Yet, it depends heavily on accurate 2D hand layout predictions for structure transformation, which can be unreliable in cases of occlusion, viewpoint ambiguity, or cluttered environments. Furthermore, it struggles to generalize to novel environments and objects, often overfitting to the training dataset. Overall, current methods lack the detailed understanding of exocentric observations necessary to synthesize precise and realistic hand-object interactions from a first-person view.

To address the limitations of current approaches, we propose *EgoWorld*, a novel framework for translating exocentric views into egocentric views using rich exocentric observations, as illustrated in Fig. 1. Our method employs a two-stage pipeline to reconstruct the egocentric view: (1) extracting diverse observations from the exocentric view, including projected point clouds, 3D hand poses, and textual descriptions; and (2) reconstructing the egocentric view based on these extracted cues. In the first stage, we construct a point cloud by combining the input exocentric RGB image with a scale-aligned estimated exocentric depth map, using the 3D exocentric hand pose for spatial calibration. This point cloud is then transformed into the egocentric view using a translation matrix computed from the predicted 3D hand poses in both views. After the projection of the point cloud, a sparse egocentric image is obtained and it is subsequently reconstructed into a dense, high-quality egocentric image using a diffusion-based model. To further enhance the semantic alignment and visual fidelity of the hand-object reconstruction, we incorporate the predicted exocentric text description and estimated egocentric hand pose during the reconstruction process.

We evaluate the effectiveness of *EgoWorld* through extensive experiments conducted on the H2O [3] and TACO [14] datasets, which provides well-annotated exocentric and egocentric video pairs. Our method achieves state-of-the-art performance on this benchmark. As a result, thanks to its end-to-end design, *EgoWorld* demonstrates strong generalization across various scenarios, including unseen objects, actions, scenes, and subjects. Furthermore, we conduct on unlabeled real-world examples, and *EgoWorld* shows powerful in-the-wild generalization, which implies *EgoWorld* can extend to real-world use cases.

Our main contributions can be summarized as follows:

- We introduce *EgoWorld*, a novel end-to-end framework that reconstructs high-fidelity egocentric views from a single exocentric image by leveraging rich multimodal cues, including projected point clouds, 3D hand poses, and textual descriptions.
- Our two-stage pipeline uniquely integrates geometric reasoning with semantic information and diffusion-based inpainting that significantly enhances hand-object interaction fidelity and semantic alignment in the synthesized egocentric images.
- We demonstrate the strong generalization capability of *EgoWorld* through extensive experiments on the H2O and TACO benchmarks. Our approach achieves state-of-the-art performance across diverse and previously unseen scenarios (*i.e.*, unseen objects, actions, scenes, and subjects).
- We show *EgoWorld*'s real-world applicability with unlabeled examples, and establish a new standard for exocentric-to-egocentric view translation.

## 2 Related Work

### 2.1 Exocentric-Egocentric Translation

Egocentric vision has also been scaling up particularly due to the introduction of benchmarks [2–4, 15–17]. Specifically, [2–4] opens up new opportunities for joint egocentric and exocentric vision with large-scale synchronized multi-view egocentric-exocentric videos with multi-modality annotations. Recently, research on exocentric-to-egocentric (and vice versa) translation [10–13, 18] has also gained significant attention. Intention-Ego2Exo [18] proposed an intention-driven ego-to-exo video generation framework that leverages head trajectory and action descriptions to guide content-consistent and motion-aware video synthesis. Exo2Ego [13] introduced a two-stage generative framework for exocentric-to-egocentric view translation that leverages structure transformation and diffusion-based hallucination with hand layout priors. 4Diff [11] proposed a 3D-aware diffusion model for translating exocentric images into egocentric views using egocentric point cloud rasterization and 3D-aware rotary cross-attention. Exo2Ego-V [10] presented a diffusion-based method for generating egocentric videos from sparse 360° exocentric views of skilled daily-life activities, addressing challenges like viewpoint variation and motion complexity. EgoExo-Gen [12] addressed cross-view video prediction by generating future egocentric frames from an exocentric video, the initial egocentric frame, and textual instructions, using hand-object interaction dynamics as key guidance. However, these works have fatal limitations: dependency of 2D layouts, pre-defined relative camera pose, multi-view or consecutive sequences inputs, and the challenge of integrating multiple external modalities, such as textual description and pose map.

### 2.2 Image Completion

Image completion is a fundamental problem in computer vision, which aims to fill missing regions with plausible contents [19–25]. For example, MAT [25] proposed a transformer-based model for large-hole image inpainting that combines the strengths of transformers and convolutions to efficiently handle high-resolution images. On the other hand, masked image encoding methods learn representations from images corrupted by masking [19, 26–30]. For example, MAE [30] masks random patches of an input image and learns to reconstruct the missing regions. However, these studies have a limitation that they rely solely on the information surrounding the pixels to restore missing area. With the advent of foundational diffusion models [9, 31], it has become possible to perform image completion based on various types of conditions. Specifically, latent diffusion model [8] supports flexible conditioning such as text or bounding boxes and enable high-resolution image synthesis, achieving state-of-the-art results in inpainting, class-conditional generation, and other tasks by incorporating cross-attention. Furthermore, the value of diffusion-based models has been demonstrated across a wide range of challenging domains, such as hand-hand or hand-object interaction image generation [32, 33], and motion generation [34, 35].

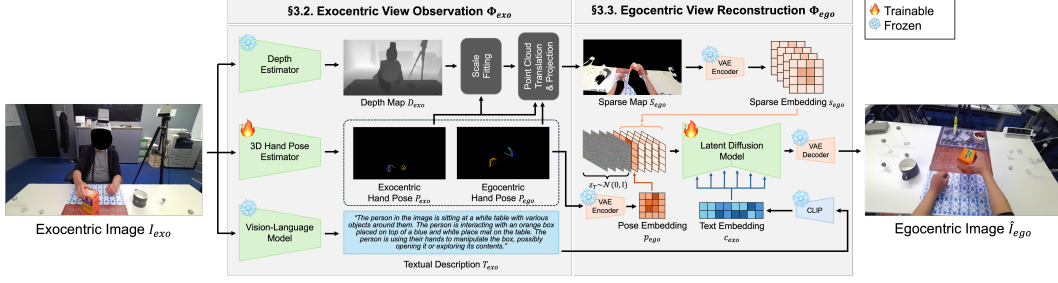


Figure 2: **Overall framework of *EgoWorld*.** *EgoWorld* has a two-stage pipeline : (1) Exocentric view observation  $\Phi_{exo}$ , which extracts diverse observations from the exocentric view, including projected point clouds, 3D hand poses, and textual descriptions; and (2) egocentric view reconstruction  $\Phi_{ego}$ , which reconstructs the egocentric view based on cues from the exocentric view observation.

## 3 Method

### 3.1 Problem Formulation

*EgoWorld* consists of two stages: exocentric view observation  $\Phi_{exo}$  and egocentric view reconstruction  $\Phi_{ego}$ , as shown in Fig. 2. First, given a single exocentric image  $I_{exo} \in \mathbb{R}^{H \times W \times 3}$ ,  $\Phi_{exo}$  predicts a corresponding sparse egocentric RGB map  $S_{ego} \in \mathbb{R}^{H \times W \times 3}$ , 3D egocentric hand pose  $P_{ego} \in \mathbb{R}^{N \times 3}$ , and a textual description  $T_{exo}$ .  $H$  and  $W$  indicates height and width of  $I_{exo}$ , and  $N$  indicates the number of keypoints of the hand. Then, in  $\Phi_{ego}$ , an egocentric image  $\hat{I}_{ego} \in \mathbb{R}^{H \times W \times 3}$  is generated based on the observations predicted in  $\Phi_{exo}$ . Therefore, *EgoWorld* is formulated as follows:

$$S_{ego}, P_{ego}, T_{exo} = \Phi_{exo}(I_{exo}), \quad (1)$$

$$\hat{I}_{ego} = \Phi_{ego}(S_{ego}, P_{ego}, T_{exo}). \quad (2)$$

### 3.2 Exocentric View Observation

Exocentric view observation  $\Phi_{exo}$  takes various real-world observations, such as sparse egocentric RGB map  $S_{ego}$ , 3D egocentric hand pose  $P_{ego}$ , and textual description  $T_{exo}$ , from the single exocentric image  $I_{exo}$ . These observations are essential for the egocentric view reconstruction  $\Phi_{ego}$ .

First, with an off-the-shelf depth estimator [36], an exocentric depth map  $D_{exo} \in \mathbb{R}^{H \times W}$  is extracted from  $I_{exo}$ . Obtaining  $D_{exo}$  is essential, because in  $\Phi_{ego}$ , the reconstruction process relies on  $S_{ego}$ , which serves as a crucial hint. Specifically, when pixel information from an exocentric view is transformed into an egocentric view, it provides partial observations of the hand, object, or scene, and this serves as a strong basis for approaching the problem from an inpainting perspective.

Next, a 3D exocentric hand pose  $P_{exo} \in \mathbb{R}^{N \times 3}$  is extracted from  $I_{exo}$  with an off-the-shelf hand pose estimator [37]. As  $D_{exo}$  provides only relative depth and is inherently affected by scale ambiguity, it is crucial to leverage  $P_{exo}$  for reasonable scale fitting. Specifically, it is possible to extract a metrically-scaled  $P_{exo}$  and an exocentric hand depth map  $D_{hand} \in \mathbb{R}^{H \times W}$  from the estimated MANO[38]-based mesh of  $P_{exo}$ . We define a hand region  $\Omega_{hand}$ , which is a pixel-level valid area determined by  $D_{hand}$ , and compute a global scale factor  $s^*$  by comparing it with  $D_{exo}$  as follows:

$$s^* = \text{median}_{(u,v) \in \Omega_{hand}} \frac{D_{hand}(u,v)}{D_{exo}(u,v) + \delta}, \quad (3)$$

where  $u, v$  indicate the pixel coordinate of depth maps, and  $\delta$  is a small constant to prevent division by zero. Applying  $s^*$  yields a metrically-calibrated exocentric depth map  $D'_{exo} = s^* D_{exo}$ . Therefore, with  $I_{exo}$  and an exocentric camera intrinsic parameter  $K_{exo} \in \mathbb{R}^{3 \times 3}$ , which is estimated from the off-the-shelf depth estimator,  $D'_{exo}$  is utilized to obtain a point cloud  $C_{exo} \in \mathbb{R}^{(H \times W) \times 6}$ .

To project  $C_{exo}$  in the egocentric view, we need an exocentric-to-egocentric view translation matrix  $X \in \mathbb{R}^{4 \times 4}$ , which can be computed through a transformation between  $P_{exo}$  and  $P_{ego}$ . However, to the best of our knowledge, there is no model which predicts  $P_{ego}$  directly from  $I_{exo}$ . Thus, we build

a powerful-but-simple 3D egocentric hand pose estimator  $\phi_{ego}$ , which is designed with a simple architecture consisting of a ViT[28]-based backbone  $\phi_{backbone}$  and an MLP-based regressor  $\phi_{reg}$ . Specifically, after extracting an image feature from  $I_{exo}$  with  $\phi_{backbone}$ , it is fed through  $\phi_{reg}$  to obtain  $P_{ego}$ . We optimize  $\phi_{ego}$  with an L2 loss function.

From the obtained  $P_{exo}$  and  $P_{ego}$ , we calculate  $X$  between them with the Umeyama algorithm [39], which estimates a transformation matrix as follows:

$$X_{ego \rightarrow exo} = (s, \mathbf{R}, \mathbf{t}), \text{ such that } P_{exo} \approx s\mathbf{R}P_{ego} + \mathbf{t}. \quad (4)$$

Here,  $s$ ,  $\mathbf{R}$ , and  $\mathbf{t}$  are the estimated scale, rotation, and translation matrices. Since both  $P_{exo}$  and  $P_{ego}$  are in metric units,  $s$  is expected to be close to 1. The transformation from exocentric to egocentric view is given by  $X = (X_{ego \rightarrow exo})^{-1}$ . Therefore, we translate  $C_{exo}$  with  $X$  into  $C_{ego}$ , project it into egocentric view with an egocentric camera intrinsic parameters  $K_{ego} \in \mathbb{R}^{3 \times 3}$ , and obtain the sparse egocentric RGB map  $S_{ego}$ .

Finally,  $T_{exo}$  is extracted with an off-the-shelf vision-language model (VLM) [40]. For example, when  $I_{exo}$  and user-provided question (i.e., “Describe in detail about the scene and the object that the person is interacting with using their hands.”) are given, VLM outputs the corresponding answer  $T_{exo}$ . Since  $T_{exo}$  contains both the overall contextual information present in the exocentric view and specific details about actions and objects, it significantly aids  $\Phi_{ego}$  for reconstructing the faithful egocentric view for unseen scenarios.

### 3.3 Egocentric View Reconstruction

From  $\Phi_{exo}$ , we obtain high-level observations  $S_{ego}$ ,  $P_{ego}$ , and  $T_{exo}$ . In  $\Phi_{ego}$ , our goal is to reconstruct a dense and reliable egocentric image  $\hat{I}_{ego}$  using them. Since  $S_{ego}$  only contains partial information observed from the exocentric view, it is necessary to reconstruct the missing regions. Thus, leveraging the powerful latent diffusion model (LDM) [8], we exploit exocentric observations  $S_{ego}$ ,  $P_{ego}$ , and  $T_{exo}$  for  $\Phi_{ego}$ .

Following the LDM, input images are encoded into the latent embedding using a frozen VAE encoder [41], and the denoised latent embedding is decoded into an output image using the frozen VAE decoder. Specifically, we encode  $S_{ego}$  to a sparse embedding  $s_{ego} \in \mathbb{R}^{64 \times 64 \times 4}$  with VAE encoder. We obtain a 2D egocentric hand pose map  $P_{ego}^{2D} \in \mathbb{R}^{512 \times 512 \times 3}$  by projecting  $P_{ego}$  with  $K_{ego}$ , encode  $P_{ego}^{2D}$  to 4-channels embedding with VAE encoder, and reduce the number of channels of 4-channels embedding to 1-channel via a channel reduction layer. This layer consists of one convolutional layer, which inputs 4-channels embedding and outputs 1-channel embedding. Therefore, we obtain a 1-channel pose embedding  $p_{ego} \in \mathbb{R}^{64 \times 64 \times 1}$ .

During training, the ground-truth egocentric image  $I_{ego} \in \mathbb{R}^{512 \times 512 \times 3}$  is also encoded to a clean latent  $z_0 \in \mathbb{R}^{64 \times 64 \times 4}$  through the VAE encoder, and the noise  $\epsilon_t \in \mathbb{R}^{64 \times 64 \times 4}$  is added to  $z_0$  to make a noisy embedding  $z_t \in \mathbb{R}^{64 \times 64 \times 4}$  with timestep  $t$  as follows:

$$z_t = \sqrt{\bar{\alpha}_t} \cdot z_0 + \sqrt{1 - \bar{\alpha}_t} \cdot \epsilon, \epsilon \sim \mathcal{N}(0, \mathbf{I}), \quad (5)$$

where  $\bar{\alpha}_t$  denotes the noise level of  $t$ . By concatenating  $s_{ego}$ ,  $p_{ego}$ , and  $z_t$ , we obtain 9-channel latent embedding  $z'_t \in \mathbb{R}^{64 \times 64 \times 9}$ , which is fed into the input of a pre-trained U-Net. Simultaneously, a textual description  $T_{exo}$  is passed through CLIP [42] to obtain a text embedding  $c_{exo} \in \mathbb{R}^{77 \times 768}$ , which serves as guidance for the U-Net of LDM. In this manner, the forward and reverse processes for denoising network  $\epsilon_\theta$  are carried out to predict  $\epsilon_t$  with the following objective:

$$\mathcal{L} = \mathbb{E}_{z_0, s_{ego}, p_{ego}, t, c_{exo}, \epsilon_t} \|\epsilon_t - \epsilon_\theta(z'_t, t, c_{exo})\|_2^2. \quad (6)$$

During sampling, we start the denoising process from a random Gaussian noise  $z_T \sim \mathcal{N}(0, \mathbf{I})$  with well-trained  $\epsilon_\theta$ . We concatenate  $z_T \in \mathbb{R}^{64 \times 64 \times 4}$  with  $s_{ego}$  and  $p_{ego}$ , and feed to  $\epsilon_\theta$  to obtain the predicted latent  $\hat{z}_0 \in \mathbb{R}^{64 \times 64 \times 4}$  by reversing the schedule in Eq. 5 at each timestep  $t \in [1, T]$ . We adopt classifier-free guidance (CFG) [43] to strengthen textual guidance as follows:

$$\epsilon_t = (1 + w) \cdot \epsilon_\theta(z_t, t, c_{exo}) - w \cdot \epsilon_\theta(z_t, t, \emptyset), \quad (7)$$

where  $w$  indicates the scaling factor in CFG, and  $\emptyset$  means unconditional. To the end, the final generated egocentric image  $\hat{I}_{ego}$  is obtained from  $\hat{z}_0$  by passing the VAE decoder.

Table 1: **Comparisons with state-of-the-arts on unseen scenarios (*i.e.*, objects, actions, scenes, and subjects) in H2O [3].** Compared to state-of-the-arts (*i.e.*, pix2pixHD [44], pixelNeRF [45], and CFLD [46]), *EgoWorld* outperforms for all unseen scenarios in all metrics (*i.e.*, FID, PSNR, SSIM, and LPIPS).

Scenarios	Unseen Objects				Unseen Actions			
Methods	FID↓	PSNR↑	SSIM↑	LPIPS↓	FID↓	PSNR↑	SSIM↑	LPIPS↓
pix2pixHD [44]	436.25	25.012	0.2993	0.6057	211.10	24.420	0.2854	0.6127
pixelNeRF [45]	498.23	26.557	0.3887	0.5372	251.76	27.061	0.3950	0.8159
CFLD [46]	59.615	25.922	0.4307	0.4539	50.953	28.529	0.4324	0.4593
<i>EgoWorld</i> (Ours)	<b>41.334</b>	<b>31.171</b>	<b>0.4814</b>	<b>0.3476</b>	<b>33.284</b>	<b>31.620</b>	<b>0.4566</b>	<b>0.3780</b>

Scenarios	Unseen Scenes				Unseen Subjects			
Methods	FID↓	PSNR↑	SSIM↑	LPIPS↓	FID↓	PSNR↑	SSIM↑	LPIPS↓
pix2pixHD [44]	490.32	18.567	0.2425	0.7290	452.13	18.172	0.3310	0.7234
pixelNeRF [45]	489.13	26.537	0.2574	0.7143	493.13	22.636	0.4135	0.6838
CFLD [46]	118.10	29.030	0.3696	0.6841	129.30	21.050	0.4001	0.6269
<i>EgoWorld</i> (Ours)	<b>90.893</b>	<b>31.004</b>	<b>0.4096</b>	<b>0.6519</b>	<b>96.429</b>	<b>24.851</b>	<b>0.4605</b>	<b>0.6188</b>

## 4 Experiments

### 4.1 Datasets

To evaluate exocentric-to-egocentric translation models including our *EgoWorld*, we select well-annotated with 3D hand poses and depth maps, time-synchronized multi-view datasets, H2O [3]. H2O has various indoor videos with 5 cameras including egocentric view, and contains diverse scenarios such as unseen objects, actions, scenes, and subjects. Following [13], we split four unseen settings to evaluate generalization as follows: (1) **unseen objects**, where we train with 6 objects and test with novel 2 objects, (2) **unseen actions**, where we train with first 80% frames and test with last 20% frames, (3) **unseen scenes**, where we train with 4 scenes and test with novel 2 scenes, and (4) **unseen subjects**, where we train with subject 1 and test with subject 2. To further demonstrate the generalizability of our method, we also evaluate it on the TACO [14] dataset. Since TACO provides hand-object interaction sequences involving 196 objects and 15 actions, we adopt an **unseen actions** scenario, which allows for a general and comprehensive evaluation of generalization performance.

### 4.2 Evaluation Metrics

Following [10, 13], we adopt extensive image quality metrics to measure reconstructed egocentric images: (1) **frechet inception distance (FID)** [47], which employs Inception-v3 [48] features to compute the distributions of generated and real images, (2) **peak signal-to-noise ratio (PSNR)**, which is a pixel-wise fidelity metric that quantifies the ratio between the maximum possible pixel value and the mean squared error (MSE) between a reconstructed image and its ground truth counterpart, (3) **structural similarity index measure (SSIM)** [49], which evaluates image similarity by comparing three components, *i.e.*, luminance, contrast, and structural information, and is designed to model human visual perception more closely, and (4) **learned perceptual image patch similarity (LPIPS)** [50], which employs a deep neural network [51] trained on human judgments to evaluate reconstruction accuracy within the perceptual domain.

### 4.3 Implementation Details

To train the egocentric view reconstruction, we fine-tune a pre-trained LDM inpainting model [8]. Based on the PyTorch Lightning framework [52], we set the training settings included a batch size of 3, a learning rate of  $1 \times 10^{-5}$ , and the AdamW optimizer [53], for a total of 5 epochs. All experiments are conducted on a single NVIDIA RTX 4090 GPU. For the datasets, on H2O, we use the ground-truth egocentric sparse maps, which are derived directly from the ground-truth exocentric depth maps and relative camera poses. On TACO, due to its inherent characteristics (*i.e.*, invisible head motions), reliable estimation of egocentric hand poses is challenging. Thus, we utilize both the ground-truth hand poses and egocentric sparse maps. The implementation details of 3D egocentric hand pose estimator will be discussed in appendix.

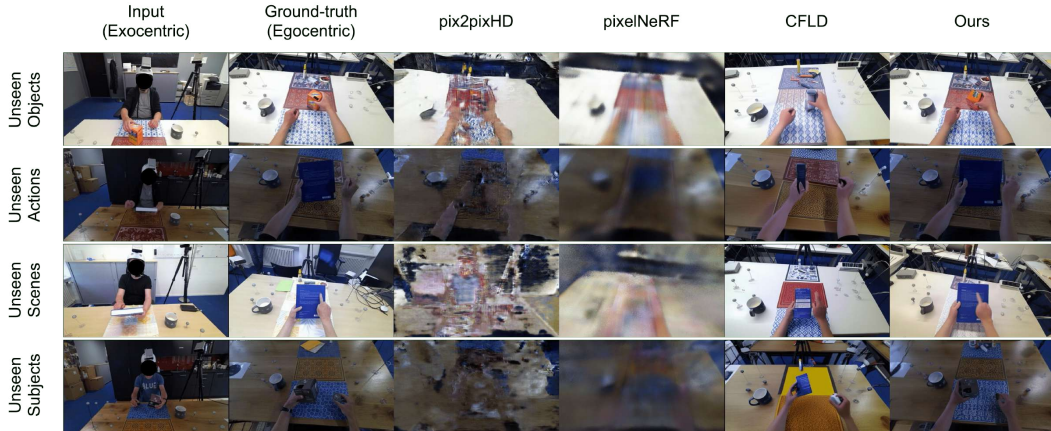


Figure 3: **Comparisons with state-of-the-arts on unseen scenarios (i.e., objects, actions, scenes, and subjects) in H2O [3].** Compared to state-of-the-arts (i.e., pix2pixHD [44], pixelNeRF [45], and CFLD [46]), *EgoWorld* outperforms the image reconstruction quality with respect to hand-object interaction and background regions for all unseen scenarios.

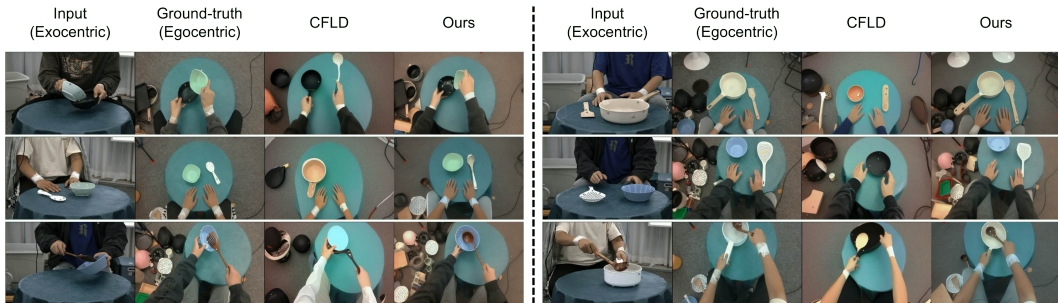


Figure 4: **Comparisons with state-of-the-art on unseen actions scenario in TACO [14].** Compared to state-of-the-art (i.e., CFLD [46]), *EgoWorld* outperforms the image reconstruction quality with respect to hand-object interaction and background regions even on more challenging scenarios than H2O [3].

## 4.4 Results

### 4.4.1 Comparisons on Benchmarks

To compare *EgoWorld* with related works, we consider several state-of-the-arts: (1) **pix2pixHD** [44], a single-view images-to-image translation model, (2) **pixelNeRF** [45], a generalizable neural rendering method that synthesizes novel views from one or few images by combining pixel-aligned features with NeRF-style volume rendering, (3) **CFLD** [46], a coarse-to-fine latent diffusion framework that decouples pose and appearance information at different stages of the generation process.

Based on experiments conducted on H2O across the 4 unseen scenarios, our method achieve state-of-the-art performance across all metrics compared to the baselines. As shown in Tab. 1, pix2pixHD and pixelNeRF show poor performance in all scenarios. CFLD, which generates view-aware person image synthesis based on a given hand pose map, demonstrates stronger performance than pix2pixHD and pixelNeRF under view changes. However, its capability is mostly limited to translating hand regions, and it performs poorly when it comes to reconstructing unseen regions such as objects and scenes. In contrast, our *EgoWorld* successfully reconstructs information observed from the exocentric view in a manner that is coherent and natural in the egocentric perspective, and outperforms all unseen scenarios in all metrics compared to state-of-the-arts. Specifically, on unseen objects scenario, *EgoWorld* shows the dramatic performance improvement compared to CFLD about 30.67%, 16.84%, 10.66%, and 23.42% of FID, PSNR, SSIM, and LPIPS, respectively. On unseen actions scenario, its improvement is about 34.68%, 9.78%, 5.30%, and 17.70% of FID, PSNR, SSIM, and LPIPS,

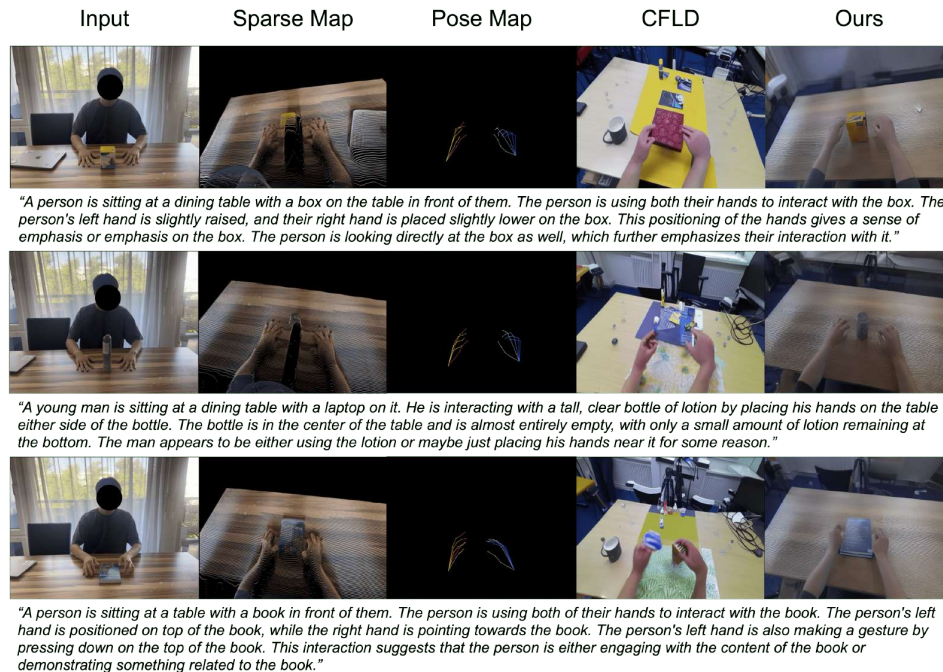


Figure 5: **Real-world comparisons with state-of-the-art.** Compared to state-of-the-art (*i.e.*, CFLD [46]), *EgoWorld* significantly outperforms with respect to hand-object interaction and background regions for in-the-wild scenarios.

respectively. On unseen scenes scenario, its improvement is about 23.04%, 6.37%, 9.77%, and 4.71% of FID, PSNR, SSIM, and LPIPS, respectively. On unseen subjects scenario, its improvement is about 25.42%, 15.30%, 13.12%, and 1.29% of FID, PSNR, SSIM, and LPIPS, respectively. In particular, the notable FID improvement is attributed to our model generating images that more closely resemble the ground-truth, especially in background regions, which occupy a large portion of the image. In contrast, the baseline model often produces backgrounds that differ significantly from the ground-truth.

As illustrated in Fig. 3, pix2pixHD produces egocentric images with noticeable noise, while pixelNeRF generates blurry outputs lacking fine details. pix2pixHD, which relies on label map-based image-to-image translation, appears unsuitable for solving the exocentric-to-egocentric view translation problem. Similarly, pixelNeRF is designed for novel view synthesis from multiple input views, making it less appropriate for the single-view to single-view translation task. In contrast, CFLD effectively reconstructs the hand pose, but fails to translate detailed information about objects and scenes, often resulting in unrealistic objects or entirely unrelated backgrounds. In comparison, *EgoWorld*, effectively leverages diverse information from the exocentric view, including pose maps, textual descriptions, and sparse maps, leading to robust performance even in challenging unseen scenarios involving complex elements like objects and scenes. More results of comparisons will be discussed in appendix.

Moreover, as illustrated in Fig. 4, *EgoWorld* demonstrates strong generalization performance even on TACO, which contains a wide variety of objects and actions compared to H2O. Unlike CFLD, which struggles to reconstruct information beyond the hand region, *EgoWorld* shows a remarkable ability to restore not only the hand but also the interacting objects and surrounding scene. These results confirm that *EgoWorld* is capable of delivering robust performance across diverse domains. More results of comparisons will be discussed in appendix.

#### 4.4.2 Comparisons on Real-World Examples

Furthermore, to evaluate in-the-wild generalization with unlabeled real-world examples, we conduct experiments on *EgoWorld* with a state-of-the-art baseline model. We take in-the-wild images of

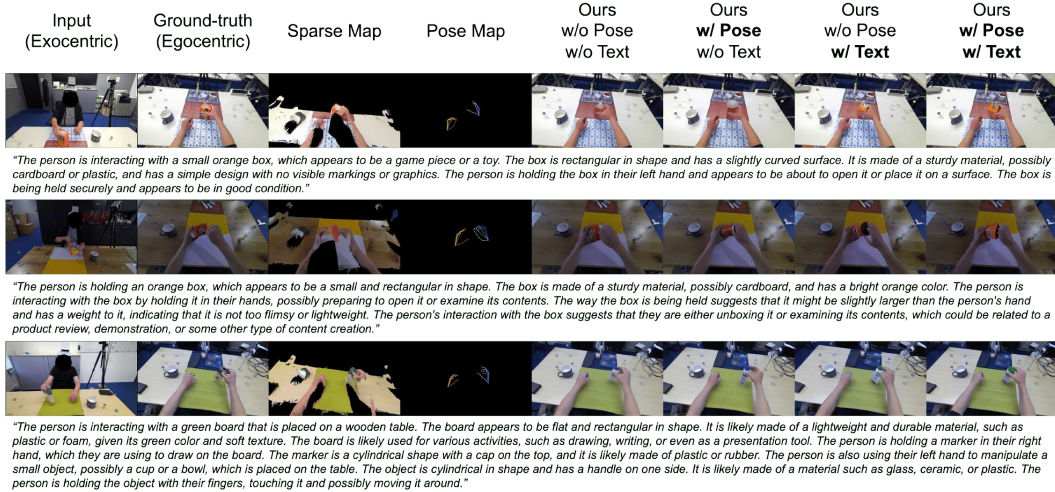


Figure 6: Comparisons on conditioning modalities of egocentric view reconstruction. *EgoWorld* generates more reasonable images when conditioned on both pose maps and text, compared to using only one or none.

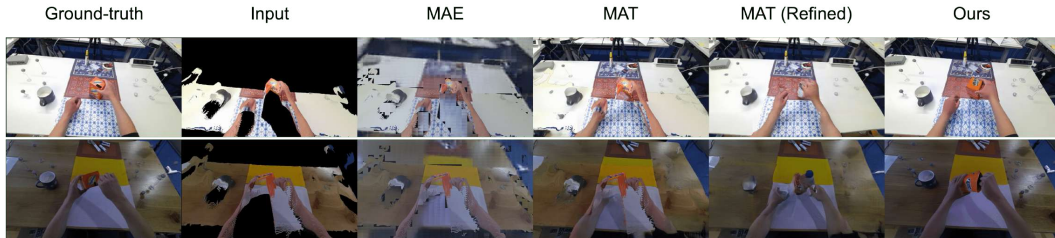


Figure 7: Results for backbones of egocentric view reconstruction. Compared to backbones (i.e., MAE [30] and MAT [25]), LDM [8] outperforms with respect to hand-object interaction and background regions for all cases.

people interacting with arbitrary objects using their hands. *Note that we rely solely on a single RGB image captured using a smartphone (iPhone 13 Pro) and apply our complete pipeline as shown in Fig. 2. No additional information beyond this single exocentric image is used.* We use pre-trained weights from our model trained on unseen action scenarios from H2O and select CFLD as the baseline, as it significantly outperforms other methods in our main experiments. As shown in Fig. 5, CFLD produces egocentric images that appear unnatural, overly biased toward training images in H2O, and are inconsistent with the new interaction scenarios. *In contrast, EgoWorld generates realistic, natural-looking egocentric views by effectively utilizing the sparse map, demonstrating strong generalization in unseen and real-world settings.* These results highlight *EgoWorld's* robustness in in-the-wild scenarios, and with further training on diverse datasets, we believe it holds strong potential for real-world applications.

#### 4.4.3 Conditioning Modalities of Egocentric View Reconstruction

*EgoWorld* reconstructs faithful egocentric images based on both the pose map and the textual description. To validate the contribution of each modality, we conduct an ablation study on it. As shown in Tab. 2, the best performance across all metrics is achieved when both pose and text information are provided. Notably, as illustrated in Fig. 6, the absence of text leads to incorrect reconstructions of unseen objects. In contrast, when text is available, the textual object information predicted from the exocentric image is effectively reflected in the egocentric view reconstruction, resulting in more plausible outputs. Additionally, the presence of hand pose information allows *EgoWorld* to produce hand configurations closer to the ground truth. These validate that *EgoWorld* performs best when leveraging both pose and textual observations.

Table 2: **Results for conditioning modalities of egocentric view reconstruction.** *EgoWorld* achieves the best scores when conditioned on both pose maps and text.

Pose	Text	FID↓	PSNR↑	SSIM↑	LPIPS↓
		56.120	27.054	0.4460	0.4454
✓		55.016	27.544	0.4449	0.4122
	✓	44.240	28.565	0.4573	0.3821
✓	✓	<b>41.334</b>	<b>31.171</b>	<b>0.4814</b>	<b>0.3476</b>

Table 3: **Results for backbones of egocentric view reconstruction.** Compared to backbones (*i.e.*, MAE [30] and MAT [25]), LDM [8] outperforms in all metrics.

Backbones	FID↓	PSNR↑	SSIM↑	LPIPS↓
MAE [30]	169.91	24.623	0.4148	0.5041
MAT [25]	89.933	28.922	0.4370	0.4758
MAT (Refined) [25]	68.628	29.750	0.4731	0.4506
LDM [8]	<b>41.334</b>	<b>31.171</b>	<b>0.4814</b>	<b>0.3476</b>

#### 4.4.4 Backbones of Egocentric View Reconstruction

Since egocentric view reconstruction closely resembles the image completion task, we compare our method with state-of-the-art image completion backbones, such as MAE [30], MAT [25], and LDM [8]. Specifically, MAE is specialized in mask-based image encoding, making it effective for filling missing pixel regions. MAT, a transformer-based model, excels at restoring large missing areas through long-range context modeling. LDM, serving as the baseline for *EgoWorld*, differs from the others in its ability to condition on diverse modalities such as text and pose. As shown in Fig. 7, our LDM-based method reconstructs egocentric view images in a more natural and high-quality manner compared to other methods. Although the vanilla MAT model performs well in filling missing areas, it often struggles to maintain consistency with the surrounding content. For example, subtle differences in table color are noticeable. To address this, we develop a refined version of MAT that uses random patch masking and recovery. However, this approach tends to fail in preserving detailed local interactions, such as hand-object interaction. In contrast, our LDM-based method, which operates by adding and removing noise in latent space, achieves coherent restoration not only in local regions but also in preserving consistency with existing areas. Moreover, as shown in Tab. 3, our approach outperforms all other methods quantitatively across all evaluation metrics. Therefore, based on these results, we adopt LDM as the backbone for *EgoWorld*.

## 5 Conclusion

In this work, we propose *EgoWorld*, a novel framework for translating exocentric observations into egocentric views using rich multi-modal exocentric cues. Our two-stage approach first extracts exocentric observations, such as projected point clouds, 3D hand poses, and textual descriptions, and then generates a realistic egocentric image from a sparse egocentric map via a diffusion model conditioned on pose and text. Extensive experiments on the H2O and TACO benchmarks validate the effectiveness and superiority of *EgoWorld*. It consistently outperforms existing baselines across various challenging scenarios, including unseen objects, actions, scenes, and subjects, for all metrics. Moreover, *EgoWorld* shows powerful generalization ability on unlabeled real-world samples compared to state-of-the-art, and it implies *EgoWorld* is enough to extend in-the-wild scenarios. These results demonstrate the potential of *EgoWorld* as a robust and versatile solution for egocentric view synthesis from exocentric inputs, paving the way for future research in cross-view understanding and generation.

**Limitations and Future Work.** While effective, *EgoWorld* depends on accurate 3D hand pose and depth estimation, which may degrade under occlusions or noise. It may also struggle with rare object categories or ambiguous pose configurations. Societal benefits include applications in assistive tech and AR, but risks involve potential privacy misuse. Safeguards like consent-aware processing and bias mitigation are essential. Future research could focus on improving the robustness of the model under challenging visual conditions, integrating temporal information from video sequences for more consistent reconstruction, and extending the framework to multi-person or multi-object interactions.

## 6 Acknowledgment

This research is funded by an SNSF Postdoc.Mobility Fellowship P500PT\_225450.

## A Appendix

In this appendix, we provide implementation details about 3D egocentric hand pose estimator to support reproducibility, additional results including 3D egocentric hand pose estimator of exocentric view observation for verifying the performance of estimator, cases of incorrect textual descriptions to evaluate the effect of text guidance, and multiple generations from the same exocentric input to evaluate consistency. We also include further examples across a variety of scenarios. Finally, we discuss additional limitations of our approach, supported by failure cases to highlight areas for future improvement.

### A.1 Implementation Details

**3D Egocentric Hand Pose Estimator.** To train a 3D egocentric hand pose estimator from exocentric inputs, we adopt a backbone as ViT-224 [28] and a regressor as MLP, which consists of two linear layers and one ReLU [54] between linear layers. The input and output feature dimensions of the first linear layer are 768 and 512, and those of the last linear layer are 512 and 126. Based on the PyTorch framework [55], we set the training settings included a batch size of 64, a learning rate of  $1 \times 10^{-4}$ , a criterion of MSE loss, and the Adam optimizer [56], for a total of 100 epochs. All experiments were conducted on a single NVIDIA RTX 4090 GPU. For the datasets, as mentioned in the main paper, we built the estimator based on H2O [3] only, not TACO [14]. Since in TACO, the subject’s head and egocentric camera are not visible from the exocentric view, it is infeasible for our estimator to obtain reliable egocentric hand poses.

### A.2 More Results

#### A.2.1 3D Egocentric Hand Pose Estimator of Exocentric View Observation

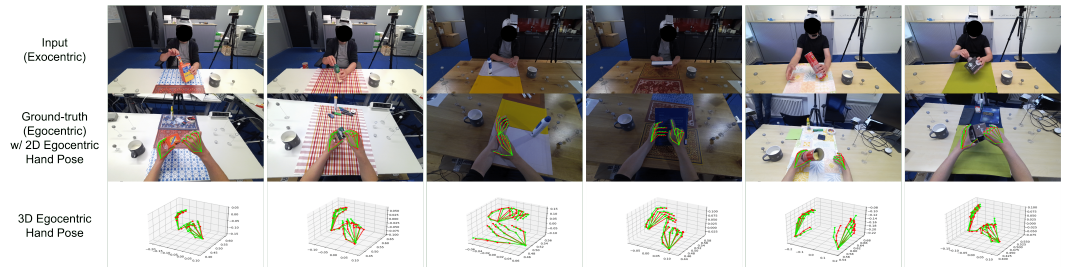


Figure A: **Results for 3D egocentric hand pose estimator.** Green and red poses indicate the ground-truth and estimated pose, respectively. Estimated poses are well-aligned with the ground-truth both in 2D and 3D spaces.

To validate the effectiveness of our newly proposed exocentric image-based 3D egocentric hand pose estimator, we conduct a qualitative analysis. As shown in Fig. A, given a single exocentric view image as input, our model predicts 3D hand poses that closely resemble the ground truth. This demonstrates that the estimator is highly useful in the exocentric view observation stage for calculating the translation matrix, as well as in the egocentric view reconstruction stage for initializing the hand pose map.

#### A.2.2 Incorrect Textual Description Guidance of Egocentric View Reconstruction

To evaluate the effect of textual description guidance of the egocentric view reconstruction, we intentionally provide an incorrect textual description that does not match the exocentric image. As shown in Fig. B, the object in the egocentric view is generated to match the object described in the description. From this result, we observe two key insights: (1) the final egocentric image can vary depending on the output of the VLM, highlighting the importance of the VLM’s performance; and (2) even when arbitrary exocentric images are fed, our model performed sufficient generalization to unseen scenarios.

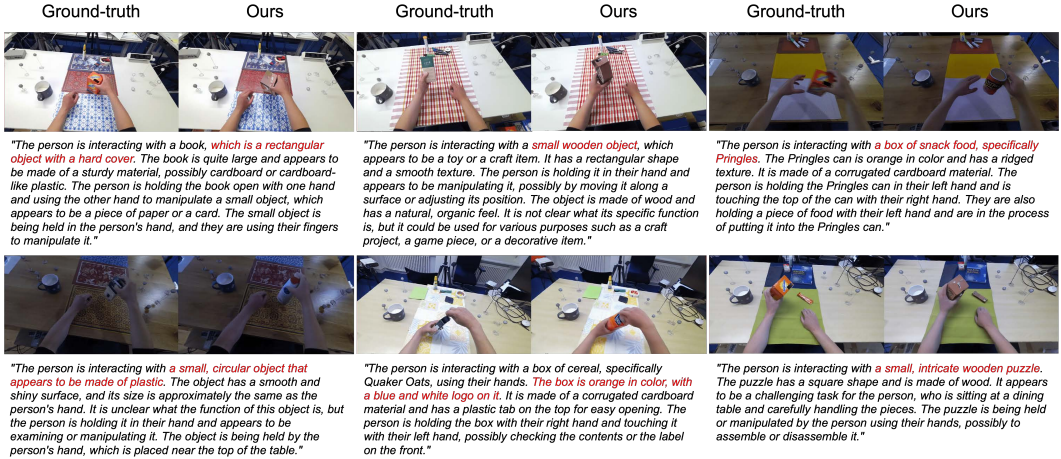


Figure B: Results for incorrect textual description guidance of egocentric view reconstruction. The red-colored texts represent incorrect descriptions, which are reflected as conditioning inputs for EgoWorld to generate egocentric images.

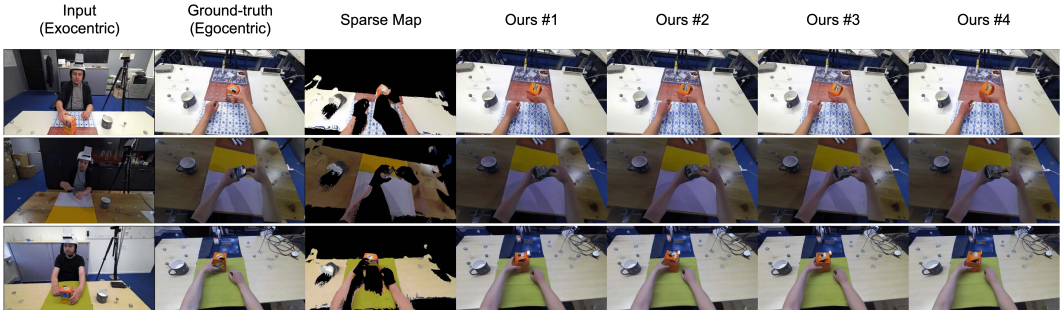


Figure C: Results for generation consistency of egocentric view reconstruction. With four iterations, the outputs are consistent, reasonable, and similar to ground-truth.

### A.2.3 Generation Consistency of Egocentric View Reconstruction

To evaluate the consistency of our generative model, we generated egocentric images multiple times under identical conditions. As shown in Fig. C, we present four outputs generated from the same exocentric image and corresponding sparse map, and our model consistently produces coherent egocentric images across runs. Despite the inherent variability in generative models, our method achieves stable and reliable exocentric-to-egocentric view translation, demonstrating its robustness and consistency.

### A.2.4 Failure Examples

In Figs. D and E, we illustrate failure examples on H2O [3] and TACO [14]. In some cases, the reconstructed hand poses or objects are different from the ground truth. For hand poses, subtle finger movements that are difficult to observe from the exocentric view are similarly hard to reproduce accurately in the egocentric view. We believe these limitations could be mitigated by developing a more advanced 3D egocentric hand pose estimator or by leveraging improved depth estimation to generate more reliable sparse maps, leading to better hand-aligned image completions. For objects, parts that are occluded or not visible in the exocentric image may appear distorted or inaccurately reconstructed in the egocentric view. Additionally, the object could be reconstructed incorrectly from the egocentric image when VLMs generates inaccurate text descriptions from the exocentric image. We anticipate that such issues can be addressed in the future with the development of more powerful VLMs.

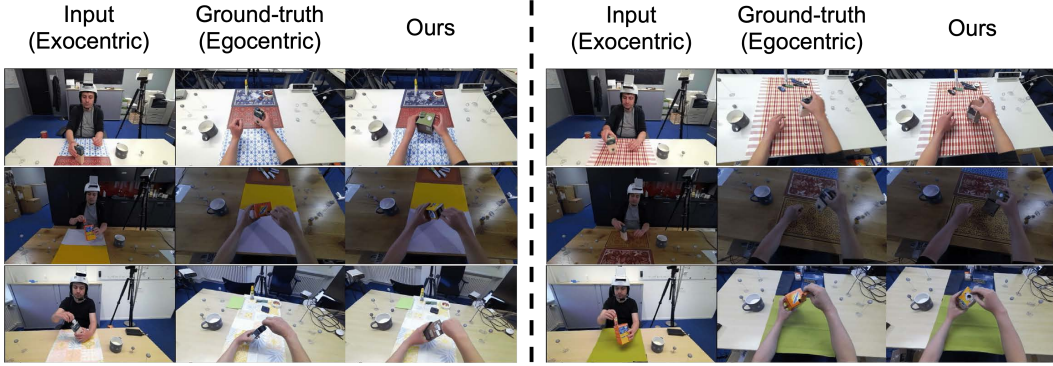


Figure D: **Results for failure examples in H2O [3].** Subtle finger movements and dependency of VLMs make the reconstructed outputs of hands and objects quite unsatisfying.

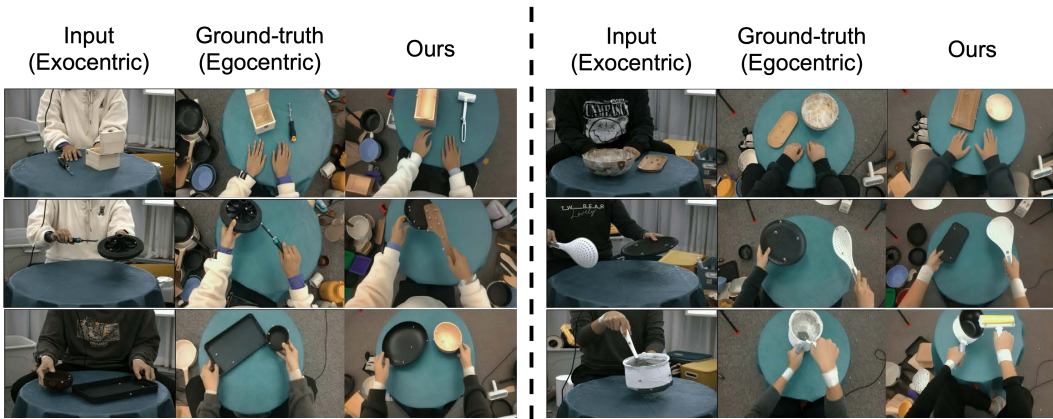


Figure E: **Results for failure examples in TACO [14].** Subtle finger movements and dependency of VLMs make the reconstructed outputs of hands and objects quite unsatisfying.

### A.2.5 Additional Comparisons with State-of-the-Arts

We provide additional state-of-the-art comparisons in this appendix as shown in Fig. F. We evaluate our method across four unseen scenarios (*i.e.*, unseen objects, actions, scenes, and subjects) and observe that it consistently outperforms baseline models. `pix2pixHD` [44], which depends on label map-based image-to-image translation, generates egocentric images with significant noise; it implies `pix2pixHD` is ill-suited for tackling the exocentric-to-egocentric view translation task. Likewise, `pixelNeRF` [45], which is originally intended for novel view synthesis using multiple inputs, produces blurry results that lack fine-grained details; it means `pixelNeRF` is less effective for one-to-one view translation. On the other hand, `CFLD` [46], which focuses on generating view-aware person images using hand pose maps, shows better performance than the previous methods. However, its strengths are largely confined to hand region translation only, and it struggles to accurately reconstruct surrounding information like objects and scenes. In contrast, our approach, *EgoWorld*, produces robust and coherent results even in complex and previously unseen scenarios involving rich contextual elements. Therefore, we verify *EgoWorld*'s generalization ability across diverse, unseen situations.

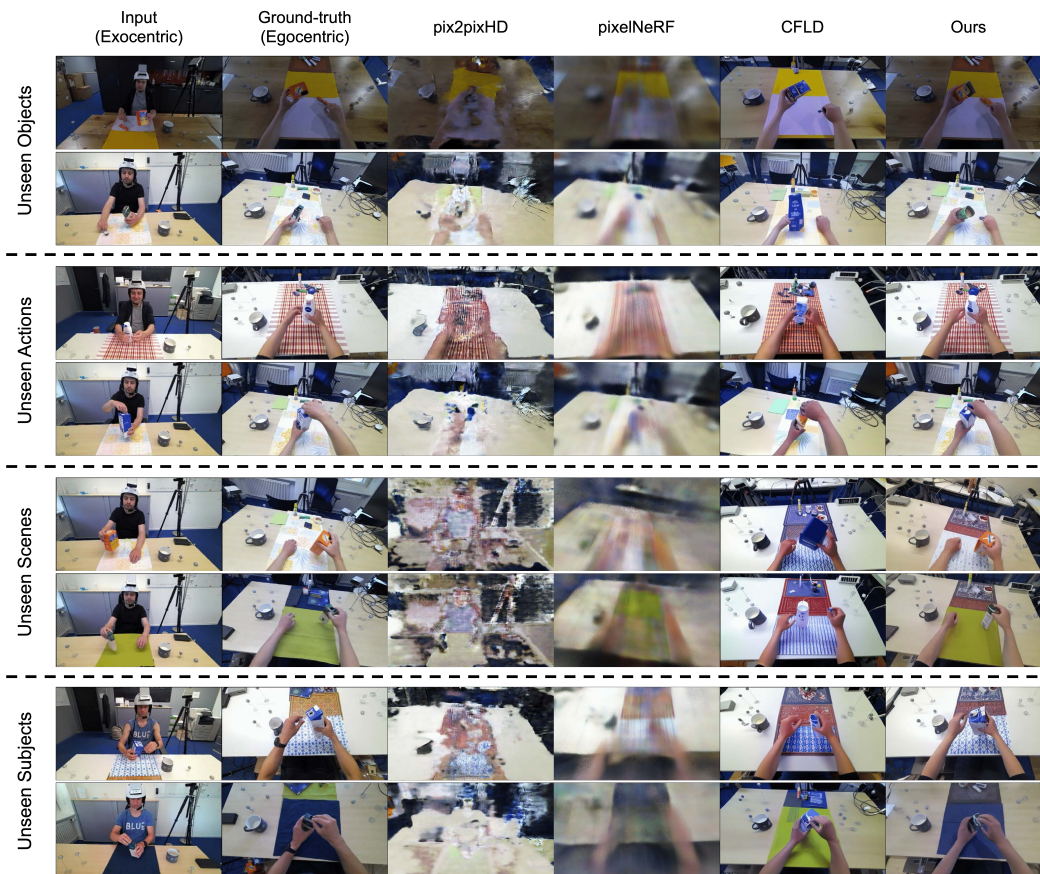


Figure F: **Results for additional comparisons with state-of-the-arts on unseen scenarios.** Compared to state-of-the-arts (*i.e.*, pix2pixHD [44], pixelNeRF [45], and CFLD [46]), *EgoWorld* outperforms for all unseen scenarios.

## References

- [1] Shervin Ardeshir and Ali Borji. An exocentric look at egocentric actions and vice versa. 171:61–68, 2018.
- [2] Kristen Grauman, Andrew Westbury, Lorenzo Torresani, Kris Kitani, Jitendra Malik, Triantafyllos Afouras, Kumar Ashutosh, Vijay Baiyya, Siddhant Bansal, Bikram Boote, et al. Ego-exo4d: Understanding skilled human activity from first-and third-person perspectives. In *CVPR*, pages 19383–19400, 2024.
- [3] Taein Kwon, Bugra Tekin, Jan Stühmer, Federica Bogo, and Marc Pollefeys. H2o: Two hands manipulating objects for first person interaction recognition. In *CVPR*, pages 10138–10148, 2021.
- [4] Fadime Sener, Dibyadip Chatterjee, Daniel Sheleпов, Kun He, Dipika Singhania, Robert Wang, and Angela Yao. Assembly101: A large-scale multi-view video dataset for understanding procedural activities. In *CVPR*, pages 21096–21106, 2022.
- [5] Benita Wong, Joya Chen, You Wu, Stan Weixian Lei, Dongxing Mao, Difei Gao, and Mike Zheng Shou. Assistq: Affordance-centric question-driven task completion for egocentric assistant. In *ECCV*, pages 485–501, 2022.
- [6] Joya Chen, Difei Gao, Kevin Qinghong Lin, and Mike Zheng Shou. Affordance grounding from demonstration video to target image. In *CVPR*, pages 6799–6808, 2023.
- [7] Difei Gao, Lei Ji, Luowei Zhou, Kevin Qinghong Lin, Joya Chen, Zihan Fan, and Mike Zheng Shou. Assistgpt: A general multi-modal assistant that can plan, execute, inspect, and learn. *arXiv preprint arXiv:2306.08640*, 2023.
- [8] Robin Rombach, Andreas Blattmann, Dominik Lorenz, Patrick Esser, and Björn Ommer. High-resolution image synthesis with latent diffusion models. In *CVPR*, pages 10684–10695, 2022.
- [9] Jonathan Ho, Ajay Jain, and Pieter Abbeel. Denoising diffusion probabilistic models. *NeurIPS*, 33:6840–6851, 2020.
- [10] Jia-Wei Liu, Weijia Mao, Zhongcong Xu, Jussi Keppo, and Mike Zheng Shou. Exocentric-to-egocentric video generation. *NeurIPS*, 37:136149–136172, 2024.
- [11] Feng Cheng, Mi Luo, Huiyu Wang, Alex Dimakis, Lorenzo Torresani, Gedas Bertasius, and Kristen Grauman. 4diff: 3d-aware diffusion model for third-to-first viewpoint translation. In *ECCV*, pages 407–425, 2024.
- [12] Jilan Xu, Yifei Huang, Baoqi Pei, Junlin Hou, Qingqiu Li, Guo Chen, Yuejie Zhang, Rui Feng, and Weidi Xie. Egoexo-gen: Ego-centric video prediction by watching exo-centric videos. In *ICLR*, 2025.
- [13] Mi Luo, Zihui Xue, Alex Dimakis, and Kristen Grauman. Put myself in your shoes: Lifting the egocentric perspective from exocentric videos. In *ECCV*, pages 407–425, 2024.
- [14] Yun Liu, Haolin Yang, Xu Si, Ling Liu, Zipeng Li, Yuxiang Zhang, Yebin Liu, and Li Yi. Taco: Benchmarking generalizable bimanual tool-action-object understanding. In *CVPR*, pages 21740–21751, 2024.
- [15] Dima Damen, Hazel Doughty, Giovanni Maria Farinella, Sanja Fidler, Antonino Furnari, Evangelos Kazakos, Davide Moltisanti, Jonathan Munro, Toby Perrett, Will Price, et al. Scaling egocentric vision: The epic-kitchens dataset. In *ECCV*, pages 720–736, 2018.
- [16] Kristen Grauman, Andrew Westbury, Eugene Byrne, Zachary Chavis, Antonino Furnari, Rohit Girdhar, Jackson Hamburger, Hao Jiang, Miao Liu, Xingyu Liu, et al. Ego4d: Around the world in 3,000 hours of egocentric video. In *CVPR*, pages 18995–19012, 2022.
- [17] Dima Damen, Hazel Doughty, Giovanni Maria Farinella, Antonino Furnari, Evangelos Kazakos, Jian Ma, Davide Moltisanti, Jonathan Munro, Toby Perrett, Will Price, et al. Rescaling egocentric vision: Collection, pipeline and challenges for epic-kitchens-100. *IJCV*, pages 1–23, 2022.
- [18] Hongchen Luo, Kai Zhu, Wei Zhai, and Yang Cao. Intention-driven ego-to-exo video generation. *arXiv preprint arXiv:2403.09194*, 2024.
- [19] Deepak Pathak, Philipp Krahenbuhl, Jeff Donahue, Trevor Darrell, and Alexei A Efros. Context encoders: Feature learning by inpainting. In *CVPR*, pages 2536–2544, 2016.
- [20] Hongyu Liu, Bin Jiang, Yi Xiao, and Chao Yang. Coherent semantic attention for image inpainting. In *ICCV*, pages 4170–4179, 2019.

- [21] Wei Xiong, Jiahui Yu, Zhe Lin, Jimei Yang, Xin Lu, Connelly Barnes, and Jiebo Luo. Foreground-aware image inpainting. In *CVPR*, pages 5840–5848, 2019.
- [22] Yuhang Song, Chao Yang, Yeji Shen, Peng Wang, Qin Huang, and C-C Jay Kuo. Spg-net: Segmentation prediction and guidance network for image inpainting. *arXiv preprint arXiv:1805.03356*, 2018.
- [23] Shengyu Zhao, Jonathan Cui, Yilun Sheng, Yue Dong, Xiao Liang, Eric I Chang, and Yan Xu. Large scale image completion via co-modulated generative adversarial networks. *arXiv preprint arXiv:2103.10428*, 2021.
- [24] Roman Suvorov, Elizaveta Logacheva, Anton Mashikhin, Anastasia Remizova, Arsenii Ashukha, Aleksei Silvestrov, Naejin Kong, Harshith Goka, Kiwoong Park, and Victor Lempitsky. Resolution-robust large mask inpainting with fourier convolutions. In *Proceedings of the IEEE/CVF winter conference on applications of computer vision*, pages 2149–2159, 2022.
- [25] Wenbo Li, Zhe Lin, Kun Zhou, Lu Qi, Yi Wang, and Jiaya Jia. Mat: Mask-aware transformer for large hole image inpainting. In *CVPR*, pages 10758–10768, 2022.
- [26] Pascal Vincent, Hugo Larochelle, Isabelle Lajoie, Yoshua Bengio, Pierre-Antoine Manzagol, and Léon Bottou. Stacked denoising autoencoders: Learning useful representations in a deep network with a local denoising criterion. *Journal of machine learning research*, 11(12), 2010.
- [27] Mark Chen, Alec Radford, Rewon Child, Jeffrey Wu, Heewoo Jun, David Luan, and Ilya Sutskever. Generative pretraining from pixels. pages 1691–1703, 2020.
- [28] Alexey Dosovitskiy, Lucas Beyer, Alexander Kolesnikov, Dirk Weissenborn, Xiaohua Zhai, Thomas Unterthiner, Mostafa Dehghani, Matthias Minderer, G Heigold, S Gelly, et al. An image is worth 16x16 words: Transformers for image recognition at scale. In *ICLR*, 2020.
- [29] Hangbo Bao, Li Dong, Songhao Piao, and Furu Wei. Beit: Bert pre-training of image transformers. *arXiv preprint arXiv:2106.08254*, 2021.
- [30] Kaiming He, Xinlei Chen, Saining Xie, Yanghao Li, Piotr Dollár, and Ross Girshick. Masked autoencoders are scalable vision learners. In *CVPR*, pages 16000–16009, 2022.
- [31] Jiaming Song, Chenlin Meng, and Stefano Ermon. Denoising diffusion implicit models. *arXiv preprint arXiv:2010.02502*, 2020.
- [32] Mengqi Zhang, Yang Fu, Zheng Ding, Sifei Liu, Zhuowen Tu, and Xiaolong Wang. Hoidiffusion: Generating realistic 3d hand-object interaction data. In *CVPR*, pages 8521–8531, 2024.
- [33] Junho Park, Kyeongbo Kong, and Suk-Ju Kang. Attentionhand: Text-driven controllable hand image generation for 3d hand reconstruction in the wild. In *ECCV*, 2024.
- [34] Junuk Cha, Jihyeon Kim, Jae Shin Yoon, and Seungryul Baek. Text2hoi: Text-guided 3d motion generation for hand-object interaction. In *CVPR*, pages 1577–1585, 2024.
- [35] Mingzhen Huang, Fu-Jen Chu, Bugra Tekin, Kevin J Liang, Haoyu Ma, Weiyao Wang, Xingyu Chen, Pierre Gleize, Hongfei Xue, Siwei Lyu, et al. Hoigt: Learning long-sequence hand-object interaction with language models. In *CVPR*, pages 7136–7146, 2025.
- [36] Jianyuan Wang, Minghao Chen, Nikita Karaev, Andrea Vedaldi, Christian Rupprecht, and David Novotny. Vggt: Visual geometry grounded transformer. *arXiv preprint arXiv:2503.11651*, 2025.
- [37] Zhengdi Yu, Shaoli Huang, Fang Chen, Toby P. Breckon, and Jue Wang. Acr: Attention collaboration-based regressor for arbitrary two-hand reconstruction. In *CVPR*, June 2023.
- [38] Javier Romero, Dimitris Tzionas, and Michael J Black. Embodied hands: Modeling and capturing hands and bodies together. *ACM TOG*, 36(6), 2017.
- [39] Shinji Umeyama. Least-squares estimation of transformation parameters between two point patterns. *IEEE TPAMI*, 13(04):376–380, 1991.
- [40] Jinze Bai, Shuai Bai, Shusheng Yang, Shijie Wang, Sinan Tan, Peng Wang, Junyang Lin, Chang Zhou, and Jingren Zhou. Qwen-vl: A versatile vision-language model for understanding, localization, text reading, and beyond. *arXiv preprint arXiv:2308.12966*, 2023.
- [41] Patrick Esser, Robin Rombach, and Bjorn Ommer. Taming transformers for high-resolution image synthesis. In *CVPR*, pages 12873–12883, 2021.

- [42] Alec Radford, Jong Wook Kim, Chris Hallacy, Aditya Ramesh, Gabriel Goh, Sandhini Agarwal, Girish Sastry, Amanda Askell, Pamela Mishkin, Jack Clark, Gretchen Krueger, and Ilya Sutskever. Learning transferable visual models from natural language supervision. pages 8748–8763, 2021.
- [43] Jonathan Ho and Tim Salimans. Classifier-free diffusion guidance. *arXiv preprint arXiv:2207.12598*, 2022.
- [44] Ting-Chun Wang, Ming-Yu Liu, Jun-Yan Zhu, Andrew Tao, Jan Kautz, and Bryan Catanzaro. High-resolution image synthesis and semantic manipulation with conditional gans. In *CVPR*, pages 8798–8807, 2018.
- [45] Alex Yu, Vickie Ye, Matthew Tancik, and Angjoo Kanazawa. pixelnerf: Neural radiance fields from one or few images. In *CVPR*, pages 4578–4587, 2021.
- [46] Yanzuo Lu, Manlin Zhang, Andy J Ma, Xiaohua Xie, and Jianhuang Lai. Coarse-to-fine latent diffusion for pose-guided person image synthesis. In *CVPR*, pages 6420–6429, 2024.
- [47] Martin Heusel, Hubert Ramsauer, Thomas Unterthiner, Bernhard Nessler, and Sepp Hochreiter. Gans trained by a two time-scale update rule converge to a local nash equilibrium. *NeurIPS*, 30:6626–6637, 2017.
- [48] Tim Salimans, Ian Goodfellow, Wojciech Zaremba, Vicki Cheung, Alec Radford, and Xi Chen. Improved techniques for training gans. *NeurIPS*, 29, 2016.
- [49] Zhou Wang, Alan C Bovik, Hamid R Sheikh, and Eero P Simoncelli. Image quality assessment: From error visibility to structural similarity. *IEEE TIP*, 13(4):600–612, 2004.
- [50] Richard Zhang, Phillip Isola, Alexei A Efros, Eli Shechtman, and Oliver Wang. The unreasonable effectiveness of deep features as a perceptual metric. In *CVPR*, pages 586–595, 2018.
- [51] Karen Simonyan and Andrew Zisserman. Very deep convolutional networks for large-scale image recognition. *arXiv preprint arXiv:1409.1556*, 2014.
- [52] William Falcon and The PyTorch Lightning team. Pytorch lightning, 2019.
- [53] Ilya Loshchilov and Frank Hutter. Decoupled weight decay regularization. *arXiv preprint arXiv:1711.05101*, 2017.
- [54] Vinod Nair and Geoffrey E Hinton. Rectified linear units improve restricted boltzmann machines. In *Proceedings of the 27th international conference on machine learning (ICML-10)*, pages 807–814, 2010.
- [55] Adam Paszke, Sam Gross, Francisco Massa, Adam Lerer, James Bradbury, Gregory Chanan, Trevor Killeen, Zeming Lin, Natalia Gimelshein, Luca Antiga, et al. Pytorch: An imperative style, high-performance deep learning library. *NeurIPS*, 32, 2019.
- [56] Diederik P Kingma and Jimmy Ba. Adam: A method for stochastic optimization. *ICLR*, 2015.